European Rotorcraft Forum

ALGORITHM FOR IDENTIFICATION OF HELICOPTER OPEN-LOOP TRANSFER FUNCTIONS AND REDUCED-ORDER MODELING

Claudio Pasquali, claudio.pasquali@uniroma3.it, Roma Tre University (Italy)
Jacopo Serafini, jacopo.serafini@uniroma3.it, Roma Tre University (Italy)
Riccardo Gori, goriccardo@gmail.com, Roma Tre University (Italy)
Riekert Leibbrandt, riekert.leibbrandt@koptergroup.de, Kopter Germany GmbH (Germany)
Massimo Gennaretti, massimo.gennaretti@uniroma3.it, Roma Tre University (Italy)

Abstract
This paper deals with the development and application of an algorithm aimed at the identification of open-loop transfer functions from closed-loop data. Particularly suited for helicopter applications, it allows the identification of the machine transfer functions even in the presence of a controller. The identification algorithm is based on the knowledge of the time histories of arbitrary external inputs and corresponding control actuation and responses. It is successfully applied to the AW-09 helicopter for the identification of the transfer functions relating pilot inputs to vehicle attitudes and kinematics. Then, from their rational approximation the time domain representation of the helicopter dynamics is achieved. The capability of the final state-space helicopter model to simulate vehicle dynamics is assessed by comparing the provided helicopter time responses to arbitrary inputs, with those obtained through the high-fidelity nonlinear solver formerly used to obtain the database for the identification of the transfer functions.

1. INTRODUCTION

Helicopter design and performance analysis are complex tasks that require the interaction of disciplines such as flight mechanics, structural analysis, aerodynamics, dynamics and control, aeroelasticity, power systems, avionics and aeroacoustics.

The project CORAL* (Comprehensive Rotorcraft Analyses Lab[1]) is aimed at the integration of all these disciplines, except for power systems and avionics, into a single easy-to-adapt and user-friendly simulation tool that allows for comprehensive analyses of conventional helicopter configurations, as well as non-conventional VTOL vehicles. Due to the aforementioned high complexity of the multi-physics interaction, complete and detailed helicopter simulation requires a relevant computational effort, which is not always compatible with the designer's activities. By accepting a limited loss of precision and detail, it is possible to greatly reduce the computational effort required for simulation through the introduction of reduced order models (ROMs) that describe the response of the whole helicopter or, depending on the specific needs, the behavior of some of its components (like, for instance, main rotor dynamics,[2] main rotor aerodynamics,[3] wake inflow[4]). These are simplified mathematical differential representations of the helicopter dynamics (more generally of the dynamics of the component under analysis) capable of reproducing the response of the machine with a considerably reduced computational effort due to the reduction of the representative dynamic states[5,6].

One of the main features of the project CORAL is the integration of the *Qopter* ROM identification tool in the comprehensive suite. It has been developed in the last years[7], and further improved within CORAL activities. It is based on the identification of the frequency response functions of the modelled system.

This work presents the definition of a new algorithm in *Qopter* capable of identifying the open-loop transfer functions of a dynamic system starting from closed-loop time domain simulations, or experiments (like in [8], where a ROM model of the helicopter is directly derived from flight data test). Indeed, due to the helicopter intrinsic dynamic instability, it is impossible to identify the frequency

*The CORAL project involves partners in Italy (Roma Tre University), Greece (National Technical University of Athens and the consulting company iWind) and Canada (Carleton University's Rotorcraft Research Group – CU) under the coordination of Kopter Germany, a member of the Leonardo Group.

response functions (and hence the reduced order model) relating pilot inputs to vehicle responses through numerical or experimental data not including the action of a control system (namely, not derived from a closed-loop system). Nevertheless, the knowledge of the transfer functions, and hence of the ROM, relating the pilot inputs to uncontrolled vehicle responses (open-loop system) can be very useful for control-law design, handling qualities assessment, as well as for training simulator development. Thus, this paper is specifically aimed at applying the new method for the identification of the open-loop transfer functions of a whole helicopter (hereinafter referred to as "naked-machine" transfer functions). The developed algorithm is applied to data concerning the AW09 high-fidelity numerical simulations performed by Kopter personnel. The corresponding identified helicopter ROM is validated by comparing its predictions of responses to arbitrary pilot inputs with those directly provided by the hi-fi solver.

Finally, it is worth noting that the proposed algorithm, although developed for rotorcraft analysis and design purposes, is still general and can be conveniently used in all those applications where the identification of unstable systems from controlled closed-loop data is necessary (see, for example, [9] or [10]).

2. THE ALGORITHM

The proposed methodology consists of three main steps to obtain the ROM of the multi-input/multi-output (MIMO) system analyzed:

- identification of transfer function matrix frequency samples from time-domain, small-perturbation responses;
- rational matrix approximation (RMA) of the sampled transfer function matrix by application of a least-square technique;
- inverse transformation to time-domain obtaining a state-space representation of the linearized model.

This work specifically focuses on the first step of the identification procedure, when a MIMO dataset is available (namely, when single-input/multi-output responses are not available, as in the case of a closed-loop system). For the next two steps the reader is addressed to available literature work.[2,3,4,7]

Figure 1 depicts the general scheme of a controlled helicopter. The identification of the open-loop transfer functions is crucial to perform flight dynamics analysis like the assessment of flying qualities, but it is a critical problem if the system is unstable. Indeed, in this case it is impossible to perform simulations concerning the response to a single input perturbation, because it is necessary to apply a controller that stabilizes the system and thus the outputs are produced by combinations of multiple inputs. Similarly, if the data come from flight test, these are necessarily affected either/both by pilot or/and stability augmentation system control multi-input action. Therefore, for both numerical and experimental available responses, the system must be identified through a technique capable to deal with MIMO systems. From the analytical point of view, considering the relationship between the closed-loop transfer function matrix, $\mathbf{F}(j\omega)$, and the open-loop transfer function matrix, $\mathbf{H}(j\omega)$, from the knowledge of the control law it is always possible to derive the latter from the former as indicated by the following expression

$$\mathbf{H}(j\omega) = \mathbf{F}(j\omega)[\mathbf{I} + \mathbf{K}(j\omega)\mathbf{F}(j\omega)]^{-1} \tag{1}$$

where $\mathbf{K}(j\omega)$ denotes the controller transfer matrix.[11] In this case, once the **F** matrix is identified, the **H** matrix is straightforwardly derived. However, the control scheme may not be known and/or may be too complex and include strongly nonlinear terms. Thus, the most general and convenient approach for the determination of naked-machine transfer functions is based on the availability of a suitable dataset of closed-loop system responses.

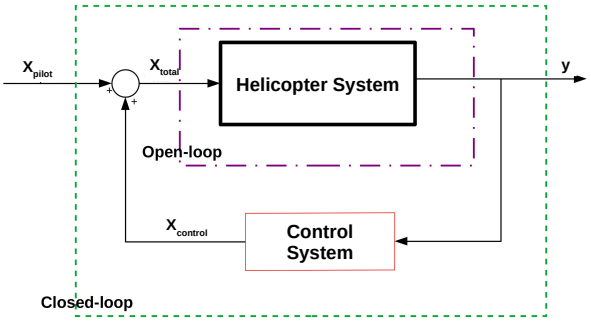

Figure 1: Helicopter block diagram representation.

Let us introduce the vector **y** as that collecting the M system outputs, and the vector **x** as that collecting the N inputs to the open-loop (naked) helicopter system deriving from the combination of pilot commands and controller feedback (namely, $\mathbf{x} \equiv \mathbf{x}_{total} = \mathbf{x}_{pilot} - \mathbf{x}_{control}$, see Fig. 1). Then, in case of noise free input/output dataset, assuming

small perturbation inputs, for each $k-$th element of the available (numerical or experimental) system database (namely, the input/output corresponding time histories $(\mathbf{x}^k, \mathbf{y}^k)$), it is formally possible to define the following relation among the components at each ω-harmonic included in the corresponding time history response

$$\tilde{\mathbf{y}}^k(j\omega) = \mathbf{H}(j\omega)\tilde{\mathbf{x}}^k(j\omega) \tag{2}$$

If, at least, N linearly independent (uncorrelated) elements of the input/output database are available, Eq. (2) can be defined N times at each harmonic of interest and all these linear equations can be combined in the following compact form

$$\mathbf{Y} = \mathbf{H}\,\mathbf{X} \tag{3}$$

with

$$\mathbf{Y} = \begin{bmatrix} \tilde{y}_1^1 & \cdots & \tilde{y}_1^N \\ \vdots & \ddots & \vdots \\ \tilde{y}_M^1 & \cdots & \tilde{y}_M^N \end{bmatrix}; \quad \mathbf{X} = \begin{bmatrix} \tilde{x}_1^1 & \cdots & \tilde{x}_1^N \\ \vdots & \ddots & \vdots \\ \tilde{x}_N^1 & \cdots & \tilde{x}_N^N \end{bmatrix} \tag{4}$$

where each column derived from one of the database elements and each row is an input/output channel. Thus, the values of the coefficients of the transfer functions at any specific harmonic are easily determined as

$$\mathbf{H} = \mathbf{Y}\,\mathbf{X}^{-1} \tag{5}$$

and this evaluation scheme is repeated for a discrete number of frequencies within the frequency range of interest for the specific application considered, in order to be ready for the second and third steps of the ROM identification process.

2.1. Database with noisy signals

Database signals (numerical or, in particular, experimental ones) may be affected by noise. In the presence of noisy signals, for each element of the database (time responses to a specific controlled perturbation input) the transfer functions can be suitably sampled by introducing the following cross-spectra

$$G_{xx}^{ni}(j\omega) = \frac{2}{T}|\tilde{x}_n^*(j\omega)\tilde{x}_i(j\omega)| \tag{6}$$

and

$$G_{xy}^{im}(j\omega) = \frac{2}{T}|\tilde{x}_i^*(j\omega)\tilde{y}_m(j\omega)| \tag{7}$$

where G_{xx}^{ni} denotes the cross-spectrum between the n-th and the i-th inputs, G_{xy}^{im} denotes the cross-spectrum between the i-th input and the m-th output, while T represents the signal observation window. Indeed, it is possible to show that, for each database element and each frequency, the $[MxN]$ transfer function matrix, $\mathbf{H}$, can be evaluated through the following relation[12]

$$\mathbf{H}^T = \mathbf{G}_{xx}^{-1}\,\mathbf{G}_{xy} \tag{8}$$

where $\mathbf{G}_{xx}$ and $\mathbf{G}_{xy}$ represent the matrices composed of the cross spectra in Eqs. (6) and (7). For the correct application of the algorithm, the complete correlation among inputs must be avoided.[13] In our problem, where the multi-input vectors, $\mathbf{x}^k$, are the result of the application of the control algorithm to the response to arbitrary perturbation inputs ($\mathbf{x}_{pilot}$ in Fig. 1), considerable correlation among inputs typically occurs.

To overcome this difficulty, in the proposed approach the transfer function matrix is determined as the output of a suitable combination of several (let us say, $K > 1$) database elements. Specifically, indicating with $\hat{\mathbf{G}}_{xx}$ and $\hat{\mathbf{G}}_{xy}$, respectively, the $[(N \times K) \times N]$ and the $[(N \times K) \times M]$ matrices obtained by sequentially ordering the rows of the $\mathbf{G}_{xx}$ and the $\mathbf{G}_{xy}$ matrices determined from the considered K different database elements, the compact form of Eq. (8) repeated for all these databases elements is given by

$$\hat{\mathbf{G}}_{xx}\,\hat{\mathbf{H}}^T = \hat{\mathbf{G}}_{xy} \tag{9}$$

where $\hat{\mathbf{H}}$ denotes the $[M \times N]$ targeted common solution matrix for the K problems in Eq. (8). Then, for each sampled frequency, from the Moore-Penrose pseudo inverse matrix, $\hat{\mathbf{G}}_{xx}^{+} = (\hat{\mathbf{G}}_{xx}^T\hat{\mathbf{G}}_{xx})^{-1}\hat{\mathbf{G}}_{xx}^T$, of the matrix $\hat{\mathbf{G}}_{xx}$ the following expression providing the transfer function matrix is determined

$$\hat{\mathbf{H}}^T = \hat{\mathbf{G}}_{xx}^{+}\,\hat{\mathbf{G}}_{xy} \tag{10}$$

which can be interpreted as the least square approximation of the unique solution of Eq. (8) written for K different database elements. It is worth noting that, although this formulation is formally equivalent to that proposed by Bendat,[12] it does not require that the inputs in each database element be linearly independent. Note also that, the minimum required value of K depends on the available $\mathbf{x}_{pilot}$ perturbations: if, for instance, each database element derives from the perturbation of a single pilot command, the definition of a well-conditioned problem is assured for $K = N$. Finally, the proposed algorithm is completed by the coherence function calculation, which is a measure of the linearity of the relation between the observed sets of outputs and inputs. For instance, considering a single-input/single-output problem, the coherence is defined as follows

(ordinary coherence)

$$\gamma_{xy}^2 = \frac{|G_{xy}|^2}{G_{xx}G_{yy}} \tag{11}$$

In the case of noise-free input, a unit coherence means that the output is fully linearly dependent on the input.

For MIMO systems, indications similar to those provided for SISO problems by the ordinary coherence are given by the multiple coherence which is defined as

$$\gamma_{x\cdot y_m}^2 = \frac{\mathbf{G}_{xy}{}^T \mathbf{G}_{xx}{}^{-1} \mathbf{G}_{xy}}{G_{yy}} \tag{12}$$

where G_{yy} is the auto-spectrum of the $\tilde{y}_m$ output. It represents the fraction of the considered output that is linearly dependent on the complete set of inputs. [14]

2.2. Reduced-order model

Following the second and third steps of the aforementioned procedure, once the transfer function matrix is suitably sampled in the range of frequency of interest, the application of a least-square procedure yields its following rational-matrix approximation (RMA) [7]

$$\mathbf{H} = s^2\mathbf{A}_2 + s\mathbf{A}_1 + \mathbf{A}_0 + \mathbf{C}[s\mathbf{I} - \mathbf{A}]^{-1}\mathbf{B} \tag{13}$$

where $\mathbf{A}_2$, $\mathbf{A}_1$, $\mathbf{A}_0$, $\mathbf{A}$, $\mathbf{B}$ and $\mathbf{C}$ are real, fully populated matrices, and s denotes the Laplace-domain variable (the degree of the polynomial contribution depends on the specific input and outputs involved in the examined problem). Matrices $\mathbf{A}_2$, $\mathbf{A}_1$ and $\mathbf{A}_0$ have dimensions $[M \times N]$, $\mathbf{A}$, is a $[P \times P]$ matrix containing the P poles of the rational expression, $\mathbf{B}$, is a $[P \times N]$ matrix, and $\mathbf{C}$ has dimensions $[M \times P]$.

Finally, recalling that the small-perturbation dynamics is described as $\tilde{\mathbf{y}} = \mathbf{H}\,\tilde{\mathbf{x}}$, combining this equation with Eq. (13) and transforming into time domain provides the following differential model that describes the system dynamics forced by an arbitrary set of inputs, through a finite number of states

$$\begin{cases} \mathbf{y} = \mathbf{A}_2\ddot{\boldsymbol{x}} + \mathbf{A}_1\dot{\boldsymbol{x}} + \mathbf{A}_0\boldsymbol{x} + \mathbf{C}\boldsymbol{r} \\ \dot{\boldsymbol{r}} = \mathbf{A}\boldsymbol{r} + \mathbf{B}\boldsymbol{x} \end{cases} \tag{14}$$

where $\boldsymbol{r}$ is the vector of the additional states introduced by the poles of the approximated transfer function matrix.

3. HIGH FIDELITY AEROMECHANIC SOLVER

The dataset available for the model identification is obtained by FlightLab [15] simulations. The computational model consists of a fully coupled, nonlinear, aerodynamic and structural solver.

The aerodynamic modelling is based on a quasi-steady strip-theory approach, with wake inflow defined through a three-state representation that includes uniform and fore-to-aft and side-to-side linear gradients. Aerodynamic loads (lift, drag, pitching moment) are derived from the sectional polar lookup tables. The structural degrees of freedom include the 6 fuselage rigid body motion DOFs, and the multiblade flap and lag hinge angles. The tail rotor blades structural DOFs are not included since the model is intended for flight dynamic purposes.

The body equations are solved in the body frame, with the body motion in the inertial frame described through the linear and angular velocity components, (u, v, w, p, q, r). The body motion in the inertial frame is obtained by integration of the body states expressed that frame through suitable rotation.

The model features a conventional control system with collective, lateral and longitudinal cyclic, and pedal control. The main rotor swash-plate routine computes the feathering angle, rate, and acceleration for each blade, starting from azimuth and rotor speed. The blade motion is imposed at the feathering hinges. Two control configurations are considered, one with and one without feedback control. The model with feedback control includes rate controllers for p, q and r, using three independent proportional and integral (PI) feedback controllers on the lateral cyclic, longitudinal cyclic and pedal channels. Feedback control is not considered for the collective pitch.

4. NUMERICAL RESULTS

The numerical investigation is dedicated to the validation of the proposed algorithm for the identification of helicopter open-loop transfer functions, starting from a database of controlled time-responses to command inputs, as those achievable from numerical simulations or in-flight data.

First, a simple case study is examined for a preliminary verification, and then the AW09 dynamics is studied.

4.1. Preliminary verification

A simple unstable analytic system is considered to prove the capability of the proposed algorithm

to capture system transfer functions starting from closed-loop controlled data. In this numerical example, the stabilization is necessary to obtain limited output, as in a real flight test would be necessary to avoid aircraft divergence from reference trajectory.

The considered system has 3 inputs collected in the vector $\mathbf{u}$, 2 outputs collected in the vector $\mathbf{y}$, and is stabilized through application of a simple proportional control law

$$\dot{\mathbf{y}} = (\hat{\mathbf{A}} - \hat{\mathbf{B}}\hat{\mathbf{K}})\mathbf{y} + \hat{\mathbf{B}}\mathbf{u} \tag{15}$$

where

$$\hat{\mathbf{A}} = \begin{bmatrix} 1.0 & -3.0 \\ 3.0 & 1.0 \end{bmatrix}$$

$$\hat{\mathbf{B}} = \begin{bmatrix} -1.7502 & -0.8314 & -1.1564 \\ -0.2857 & -0.9792 & 0.0 \end{bmatrix} \tag{16}$$

$$\hat{\mathbf{K}} = \begin{bmatrix} -0.4453 & 0.2604 \\ 0.1299 & -1.1993 \\ -0.3706 & 0.4681 \end{bmatrix}$$

note that, the open-loop transfer function matrix of the uncontrolled system ($\hat{\mathbf{K}} = \mathbf{0}$ in Eq. (15)) is given by

$$\mathbf{H} = (s\mathbf{I} - \hat{\mathbf{A}})^{-1}\hat{\mathbf{B}} \tag{17}$$

whereas the closed-loop transfer function matrix is expressed as

$$\mathbf{F} = [(s\mathbf{I} - (\hat{\mathbf{A}} - \hat{\mathbf{B}}\hat{\mathbf{K}})]^{-1}\hat{\mathbf{B}} \tag{18}$$

and that the relation in Eq. (1) holds between them. However, it is interesting to observe that the closed-loop system output can be expressed either as

$$\tilde{\mathbf{y}} = \mathbf{F}\,\tilde{\mathbf{u}} \tag{19}$$

or as

$$\begin{aligned} \tilde{\mathbf{y}} &= (s\mathbf{I} - \hat{\mathbf{A}})^{-1}\hat{\mathbf{B}}\,(-\hat{\mathbf{K}}\tilde{\mathbf{y}} + \tilde{\mathbf{u}}) \\ &= \mathbf{H}\,(-\hat{\mathbf{K}}\tilde{\mathbf{y}} + \tilde{\mathbf{u}}) \end{aligned} \tag{20}$$

Therefore, the open-loop (naked machine) transfer function matrix can be determined in two ways: (i) through the application of Eq. (1), when the control matrix $\hat{\mathbf{K}}$ is known, once $\mathbf{F}$ is determined by an expression equivalent to that in Eq. (5), based on the knowledge of 3 suitable sets of responses $(\mathbf{y}^k, \mathbf{x}^k)$, with $\tilde{\mathbf{x}}^k = \tilde{\mathbf{u}}^k$; (ii) through direct application of Eq. (5) based on the knowledge of 3 suitable sets of responses $(\mathbf{y}^k, \mathbf{x}^k)$, with $\tilde{\mathbf{x}}^k = -\hat{\mathbf{K}}\tilde{\mathbf{y}}^k + \tilde{\mathbf{u}}^k$. note that, for our helicopter problem, the former approach would require the knowledge of only $\mathbf{x}_{pilot}$ time histories, in addition to the control law. Instead, in the latter the control law is not needed, but the knowledge of both $\mathbf{x}_{pilot}$ and $\mathbf{x}_{control}$ is required. As explained above, this is the approach developed and applied in this work.

The introduced simple system in Eq. (15) is used to prove the equivalence of the two $\mathbf{H}$-matrix identification algorithms just described and, at the same time, assess the capability of the approach proposed here for helicopter dynamics applications. Indeed, the equivalence is demonstrated in Fig. 2, where the H_{11} transfer functions determined by the two outlined procedures are compared ("OPEN LOOP" result refers to the first approach requiring the control law knowledge).

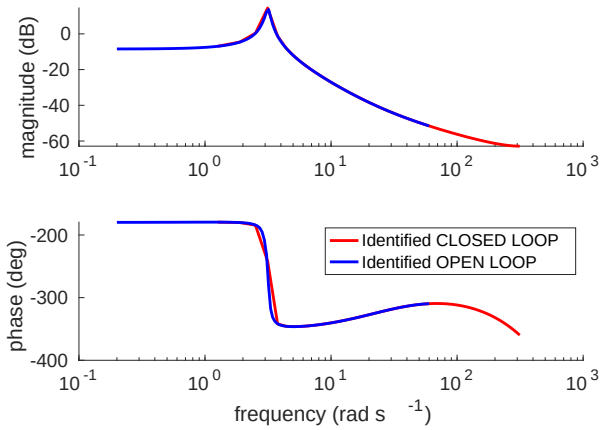

Figure 2: Comparison between transfer functions identified through different algorithms.

Indeed, the two identified transfer functions are in excellent agreement, and the same is obtained for the rest of the transfer functions that compose matrix $\mathbf{H}$ (not shown here, for the sake of conciseness).

4.2. The test case

The test case examined for algorithm validation is the flight dynamics of the AW09 (see Fig. 3) in forward flight. The main characteristics of this helicopter are reported in Tab. 1. The linearized model to be identified is a standard helicopter dynamics representation model, consisting of 4 inputs and 9 outputs.[16] The four inputs are the pilot controls, namely collective, longitudinal and lateral cyclic pitch, and pedal (θ_0,θ_s,θ_c,θ_p), whereas the outputs are the linear velocities (u, v, w), the angular velocities (p, q, r), and the helicopter attitude angles (Φ, Θ, Ψ).

mass	2500 kg
MR type	articulated
MR radius	5.5 m
MR number of blades	5
TR radius	0.6 m
TR number of blades	10

Table 1: AW09 main characteristics.

Figure 3: Leonardo Helicopter AW09.

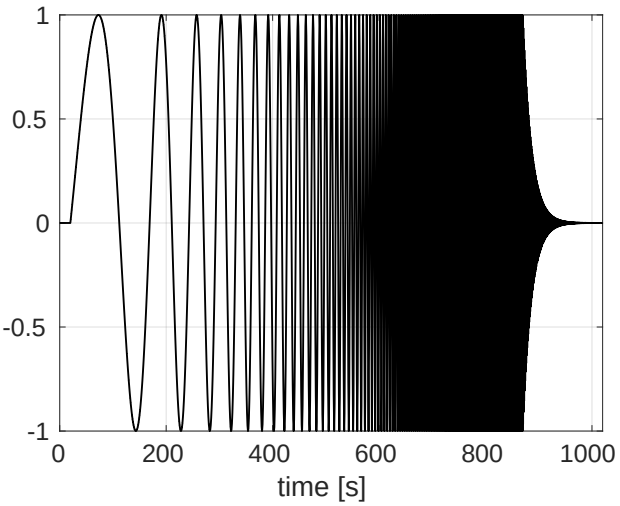

Figure 4: Chirp signal used for system identification.

The trim speed is 60 kn, and the dataset used for the identification of the transfer function matrix consists of a set of responses to chirp perturbations (see Fig. 4) of the pilot inputs that are applied while keeping the stability augmentation system active. Although one command at a time is perturbed, the actuated control produces perturbations to all commands, and hence the response is generated by a full input vector, $\mathbf{x} \equiv \mathbf{x}_{total}$. The frequency range of interest for the frequency response is that between 0.2 rad/s and 8 rad/s.

The state-space ROM obtained following the procedure described in Sec. 2 is validated through comparisons of the simulated responses to arbitrary inputs with those evaluated by FligthLab (see Sec. 3). The comparisons are accomplished for both uncontrolled and controlled helicopter, in terms of both model outputs and reconstructed perturbation trajectory (determined by integration of the flight dynamics equations for vehicle velocity in the Earth frame of reference[16]).

The arbitrary input applied for the simulations is the following mono-harmonic, windowed signal

$$y(t) = A * sin(\omega t)[H(t) - H(t - 2\pi/\omega)] \tag{21}$$

where $\omega = 1.3$ rad/s and two different amplitudes ($A = 0.5\,\text{deg}$ and $A = 1\,\text{deg}$) are used in order to verify the limitation of the linearized helicopter model accuracy with respect to input amplitude.

4.2.1. Helicopter transfer functions

As the first step of the model identification procedure is the identification of the transfer functions of the uncontrolled (naked) helicopter that appear in matrix **H**, Figs. 5 to 8 show the comparisons between some identified transfer functions and their RMA described in Eq. (13) (for the sake of conciseness, only a subset of transfer functions is depicted, with the remaining ones presenting similar quality of comparison between identified curve and RMA). Specifically, these figures consider the longitudinal dynamics frequency responses of the uncontrolled helicopter (velocity components, u,w, pitching angular velocity, q, and pitch angle, Θ) to the commands θ_0 and θ_s. They show a very good agreement between identified and approximated transfer functions both in terms of magnitude and phase, except for those that are clearly negligible (note that the magnitude is expressed in dB), thus confirming the good accuracy of the RMA algorithm.

4.3. Uncontrolled response

The validation of the ROM identified from closed-loop data begins with the analysis of the time response of the uncontrolled machine to an arbitrary input.

One single pilot command is perturbed in each test. Two different amplitudes of the perturbation are considered, one is twice the other. The comparisons between analytical ROM predictions and high-fidelity numerical simulations are given in terms of data normalized with respect to the maximum value of the considered set of curves (thus, all the graphs range is $[-1 \;:\; 1]$). For the sake of conciseness, not the whole set of validations is shown, but those presented are results representative of the overall quality of the simulations. In particular, Fig. 9 and Fig. 10 depict the helicopter response to θ_0 in terms of linear and angular velocities, respectively,

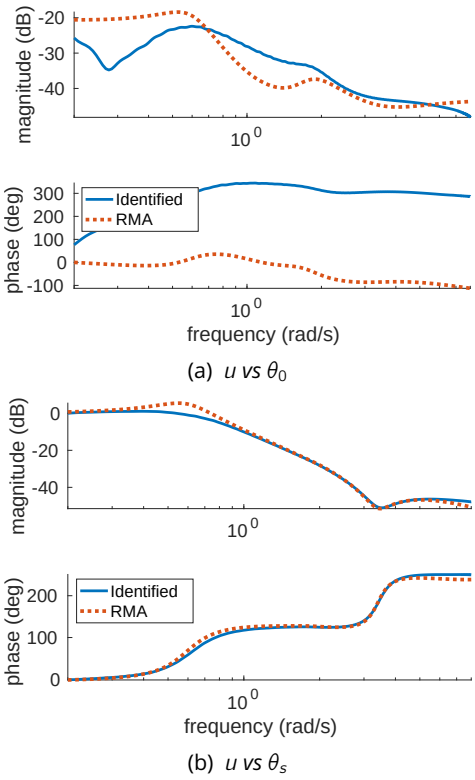

(a) u *vs* θ_0

(b) u *vs* θ_s

Figure 5: Helicopter transfer functions for u.

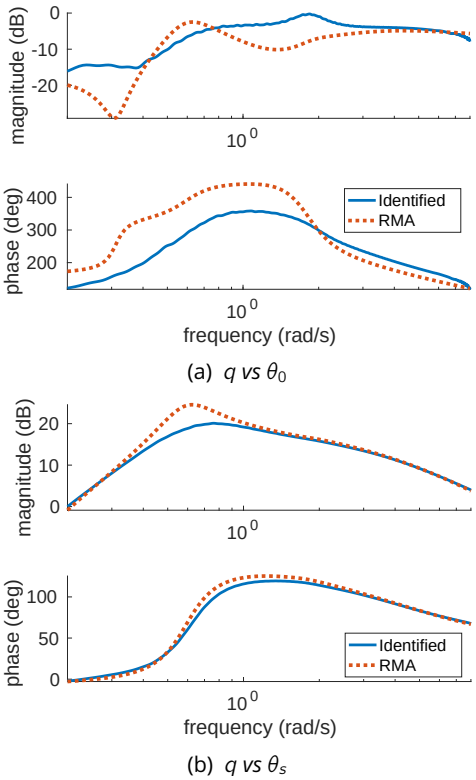

(a) q *vs* θ_0

(b) q *vs* θ_s

Figure 7: Helicopter transfer functions for q.

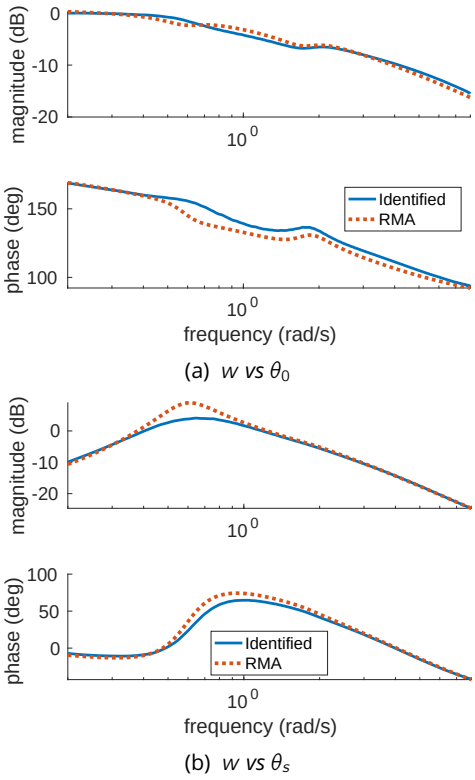

(a) w *vs* θ_0

(b) w *vs* θ_s

Figure 6: Helicopter transfer functions for w.

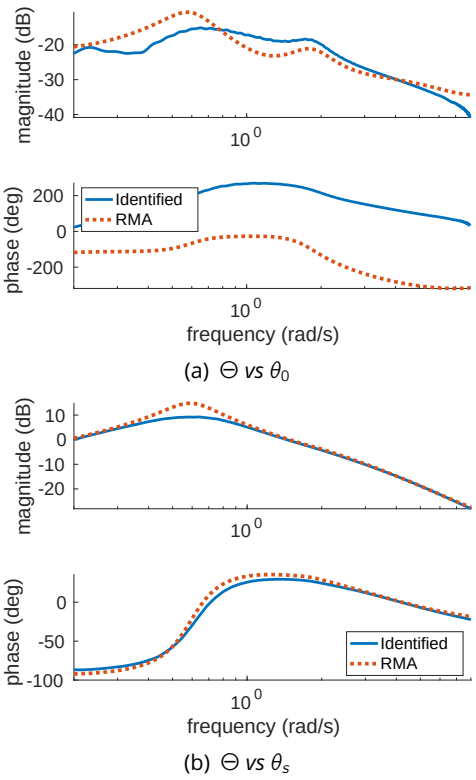

(a) Θ *vs* θ_0

(b) Θ *vs* θ_s

Figure 8: Helicopter transfer functions for Θ.

whereas Fig. 11 shows the angular velocities produced by θ_c perturbations. These results demonstrate a quite satisfactory agreement between ROM predictions and high-fidelity simulations, particularly (as expected) for the smallest input perturbations and the greatest amplitude responses.

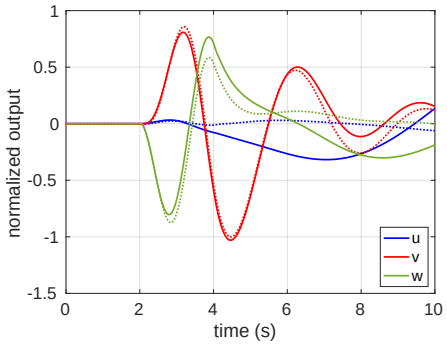

(a) *small perturbations*

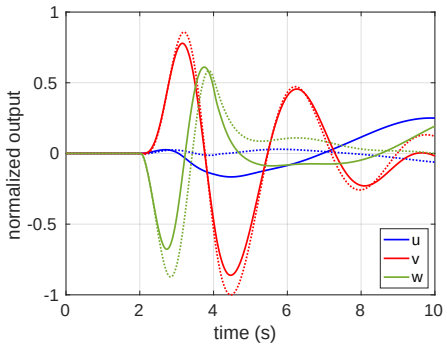

(b) *not-small perturbations*

Figure 9: Uncontrolled helicopter responses to θ_0; solid: from RMA, dashed: from FlightLab.

Then, the predicted kinematic variables are integrated to determine the corresponding trajectory perturbations, which are compared with those given by FlightLab. The comparisons in Figs. 12 to 15 show that, regardless the input amplitude, the trajectory deviation produced by θ_s perturbations are quite satisfactorily predicted by the ROM tool, whereas remarkable discrepancies between the two solutions arise for collective pitch perturbations. These are due to the ROM inaccurate capturing of the unstable helicopter dynamics that severely affects the trajectory reconstruction. After an initial good agreement, the two solutions start diverging differently form the trim solution.

4.4. Controlled Case

Next, the response of the identified helicopter subject to a controller action is examined. Two different input perturbation amplitudes and two different control gains are analyzed. The first set of control gains used are those applied for evaluating the

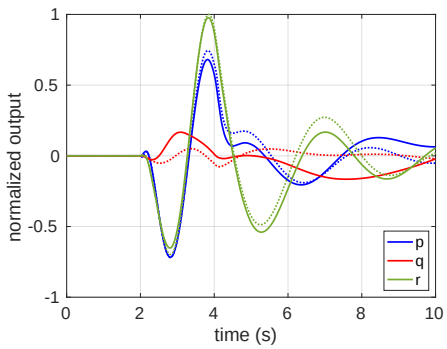

(a) *small perturbations*

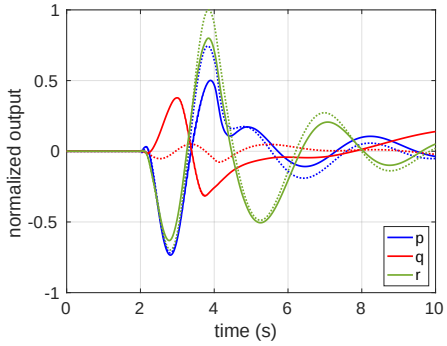

(b) *not-small perturbations*

Figure 10: Uncontrolled helicopter responses to θ_0; solid: from RMA, dashed: from FlightLab.

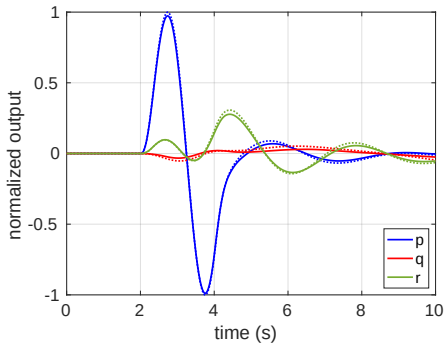

(a) *small perturbations*

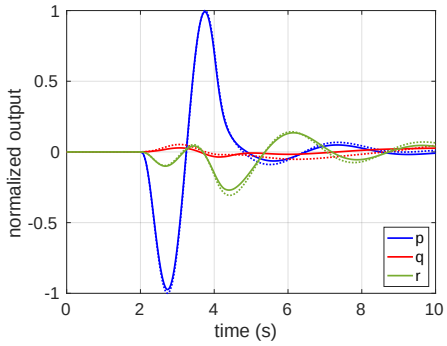

(b) *not-small perturbations*

Figure 11: Uncontrolled helicopter responses to θ_c; solid: from RMA, dashed: from FlightLab.

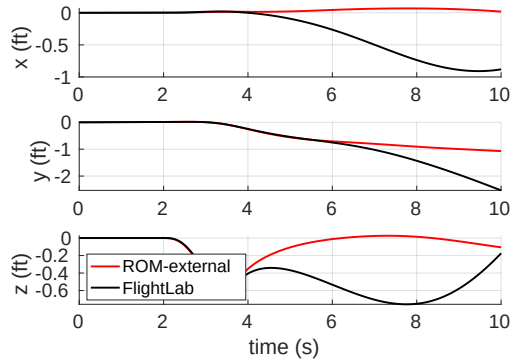

Figure 12: Uncontrolled helicopter, trajectory response to θ_0, small perturbation input.

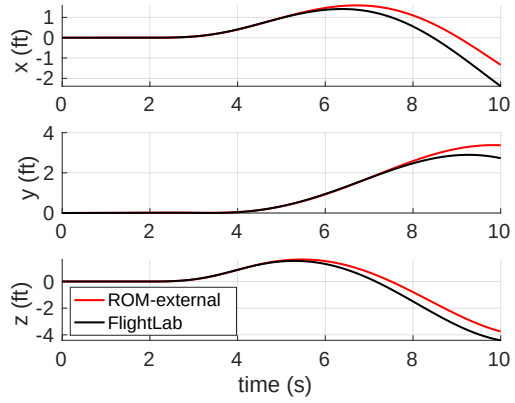

Figure 13: Uncontrolled helicopter, trajectory response to θ_s, small perturbation input.

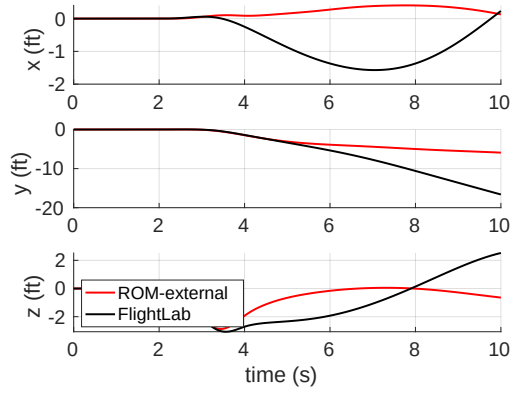

Figure 14: Uncontrolled helicopter, trajectory response to θ_0, not-small perturbation input.

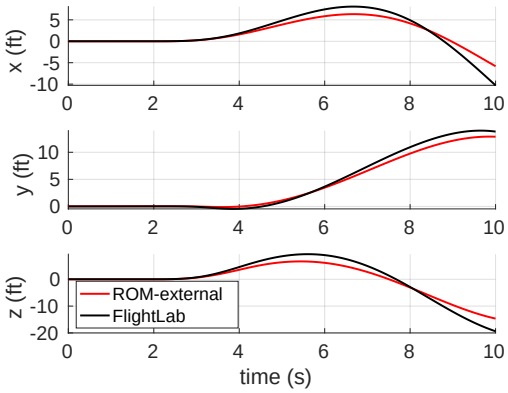

Figure 15: Uncontrolled helicopter, trajectory response to θ_s, not-small perturbation input.

database responses (referred to as normal gain), whereas the second set of gains is ten times smaller then the first one (referred to as low gain). As for the uncontrolled vehicle, ROM predictions are compared to FlightLab simulations both in terms of kinematic variables and trajectories.

4.4.1. Normal Gain

The kinematic outputs obtained for the controlled helicopter with normal gain are presented in Figs 16 to 18, whereas the corresponding trajectory perturbations are depicted in Figs. 19 to 22. In the overall, it is clearly observed that in the presence of a controller, the ROM-based simulations are in very good agreement with FlightLab predictions, showing an accuracy that is much better than that proven for the uncontrolled case.

Specifically, the kinematic components (linear and angular velocities) are almost perfectly reproduced by the ROM-based predictions for small perturbation inputs (particularly significant is the improved prediction of the u perturbation due to the collective pitch input, see Fig. 9 and Fig. 16), whereas some discrepancies arise for not-small collective pitch inputs (which, however, has to be considered as an out-of-design application of the ROM approach).

Regarding the trajectory perturbation prediction, in the case of controlled helicopter the ROM-based solution is in quite good agreement with that given by FlighLab, regardless amplitude and type of the considered perturbations. In particular, the two results almost perfectly match in terms of prediction of the z-component of the trajectory. However, it is very interesting to observe that the same quality of unsteady dynamics control is achieved by both RMA and FlightLab simulations. Indeed, this imply that the ROM tool can be effectively applied for the

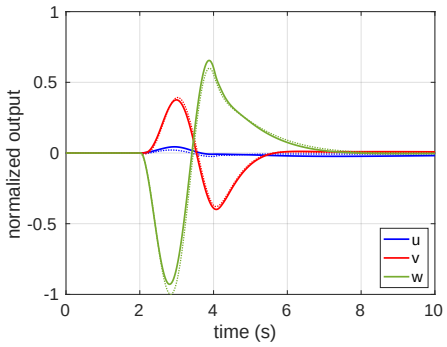

(a) *small perturbations*

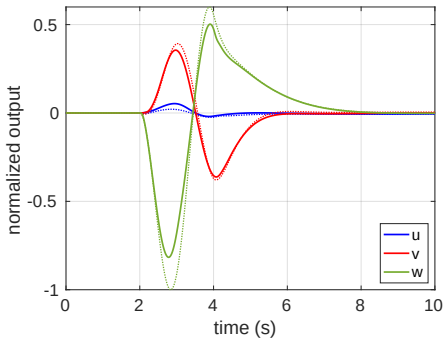

(b) *not-small perturbations*

Figure 16: Normal-gain, controlled helicopter responses to θ_0; solid: from RMA, dashed: from FlightLab.

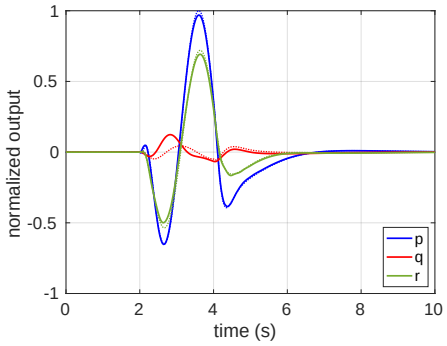

(a) *small perturbations*

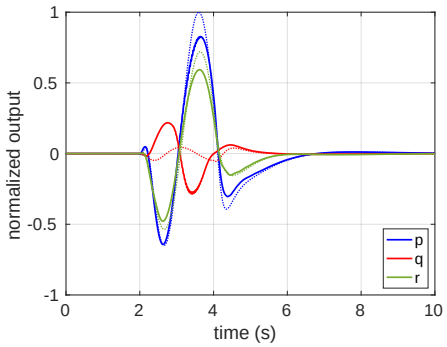

(b) *not-small perturbations*

Figure 17: Normal-gain, controlled helicopter responses to θ_0; solid: from RMA, dashed: from FlightLab.

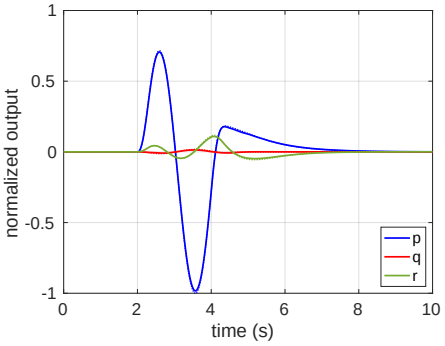

(a) *small perturbations*

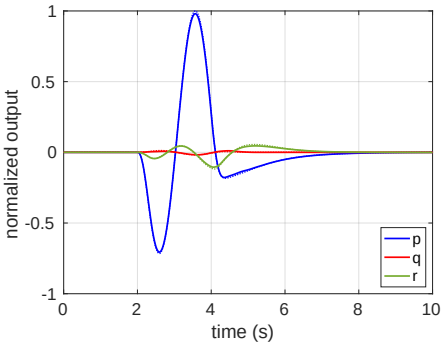

(b) *not-small perturbations*

Figure 18: Normal-gain, controlled helicopter responses to θ_c; solid: from RMA, dashed: from FlightLab.

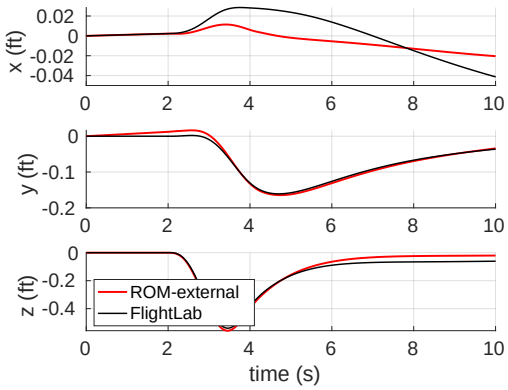

Figure 19: Normal-gain controlled helicopter, trajectory response to θ_0, small perturbation input.

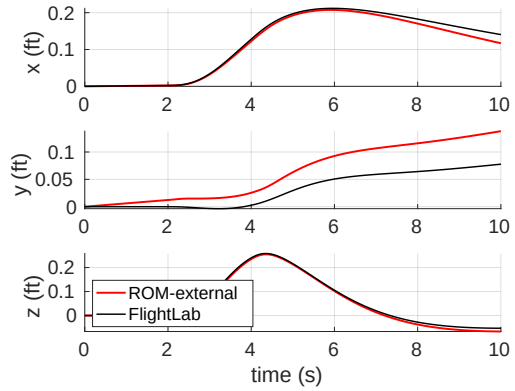

Figure 20: Normal-gain controlled helicopter, trajectory response to θ_s, small perturbation input.

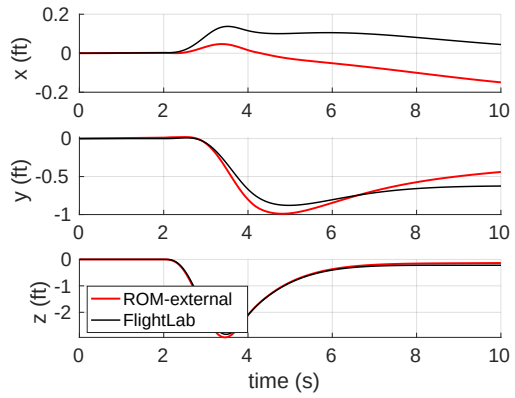

Figure 21: Normal-gain controlled helicopter, trajectory response to θ_0, not-small perturbation input.

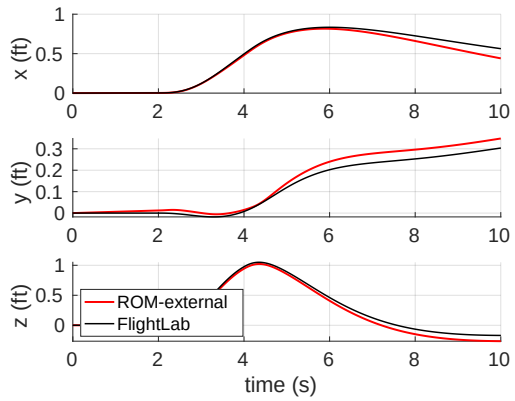

Figure 22: Normal-gain controlled helicopter, trajectory response to θ_s, not-small perturbation input.

design of reliable control laws.

4.4.2. Low Gain

The predicted helicopter kinematic responses with low-gain control actuation are presented in Figs. 23 to 25, whereas the corresponding trajectory perturbations are depicted in Figs. 26 to 31.

As mentioned above, the applied gains are $1/10$ of the gains used in the previous normal-gain results. The objective is the assessment of the reliability the ROM helicopter description by verification of its prediction capability in the presence of a controller significantly different from that applied for the evaluations of the database used in the identification process.

In the overall, the ROM-based predictions are confirmed to be in good agreement with Flightlab simulations (particularly when related to small-perturbation inputs). The most significant discrepancies appear in the predictions of trajectory perturbations due to collective pitch.

It is worth noting that for both predictions, as expected, the application of reduced values of gains yields less damped (although stabilized) system kinematic outputs, that present a more wavy behaviour than in the normal-gain control case (see, for instance, Figs. 16 and 23).

5. CONCLUSIONS

The algorithm for open-loop transfer functions identification from closed-loop data has been successfully developed and applied to determine the reduced-order model of the AW-09 helicopter dynamics. It is particularly suitable for unstable machines modelling, whose identification is necessarily accomplished through availability of a database composed of controlled machine responses. The proposed approach allows filtering the controller feedback, thus providing the open-loop transfer functions of the dynamic system. For the presented numerical investigations, the helicopter transfer functions and the corresponding ROM are determined starting from a database of responses to chirp perturbations of the pilot commands obtained through application of the high-fidelity solver FlightLab. The assessment of the accuracy of the identified helicopter model is accomplished by comparing its prediction of vehicle kinematics and trajectory perturbations due to arbitrary pilot commands with the simulations provided directly by FlightLab. The responses are examined for uncontrolled helicopter and helicopter controlled through two different gains. While the agreement between ROM

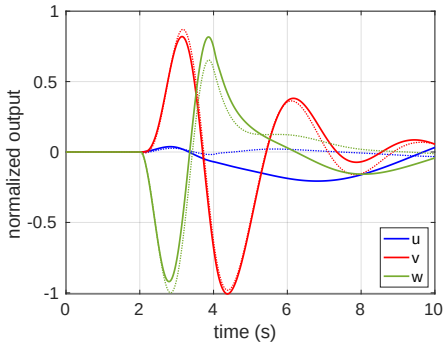

(a) *small perturbations*

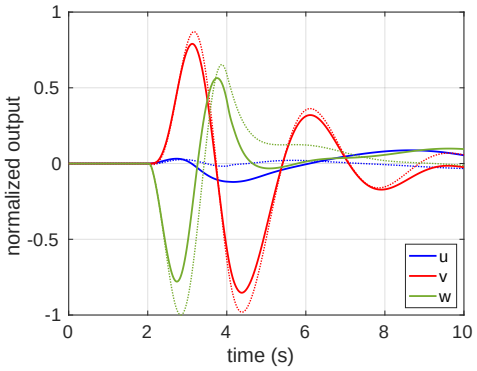

(b) *not-small perturbations*

Figure 23: Low-gain, controlled helicopter responses to θ_0; solid: from RMA, dashed: from FlightLab.

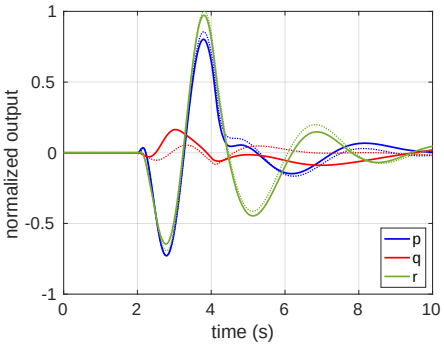

(a) *small perturbations*

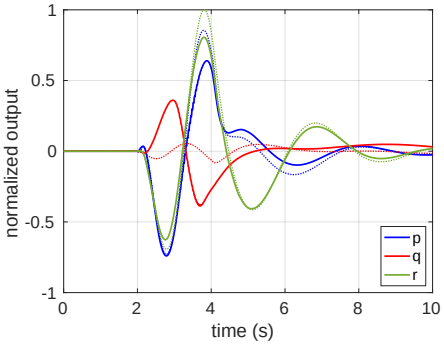

(b) *not-small perturbations*

Figure 24: Low-gain, controlled helicopter responses to θ_0; solid: from RMA, dashed: from FlightLab.

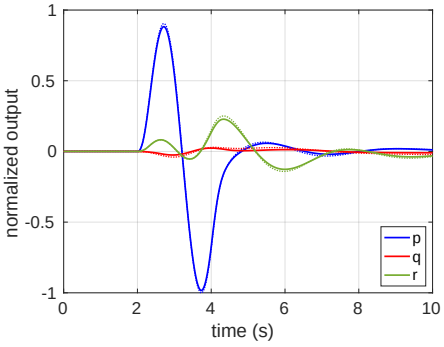

(a) *small perturbations*

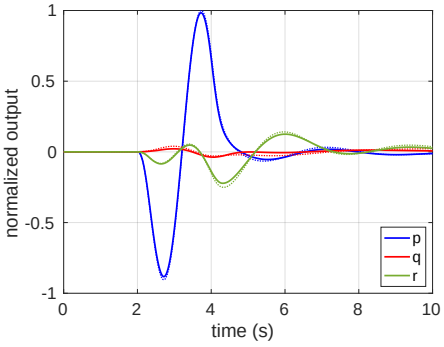

(b) *not-small perturbations*

Figure 25: Low-gain, controlled helicopter responses to θ_c; solid: from RMA, dashed: from FlightLab.

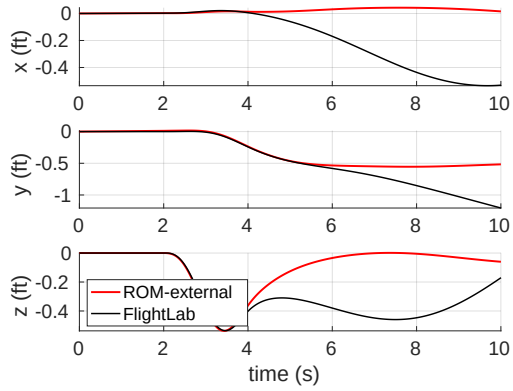

Figure 26: Low-gain controlled helicopter, trajectory response to θ_0, small perturbation input.

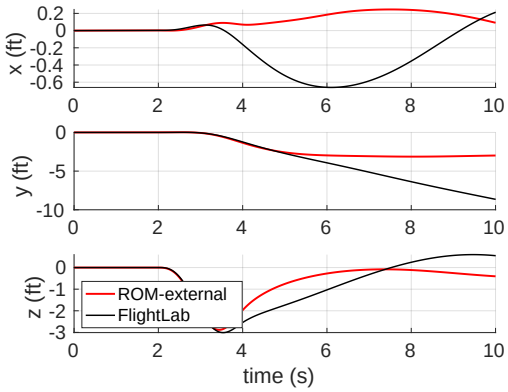

Figure 29: Low-gain controlled helicopter, trajectory response to θ_0, not-small perturbation input.

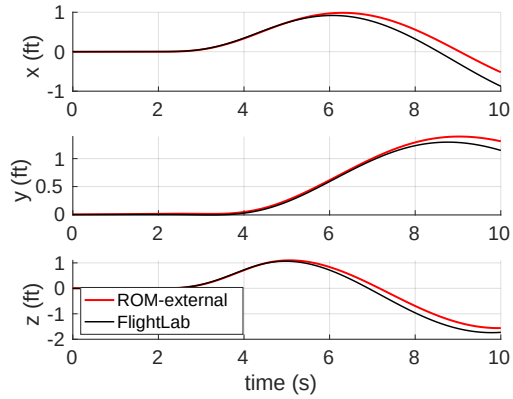

Figure 27: Low-gain controlled helicopter, trajectory response to θ_s, small perturbation input.

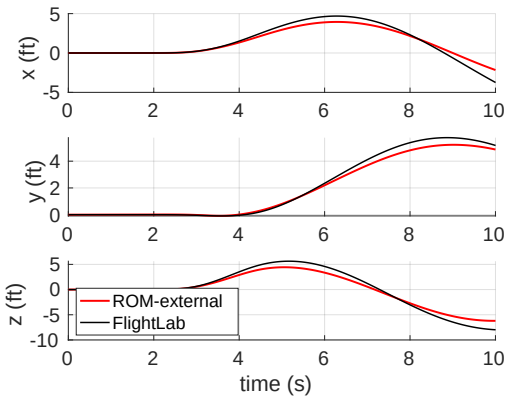

Figure 30: Low-gain controlled helicopter, trajectory response to θ_s, not-small perturbation input.

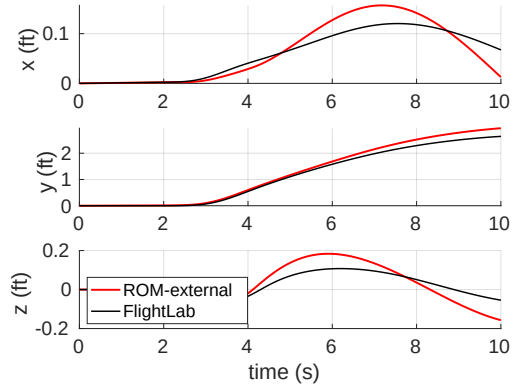

Figure 28: Low-gain controlled helicopter, trajectory response to θ_c, small perturbation input.

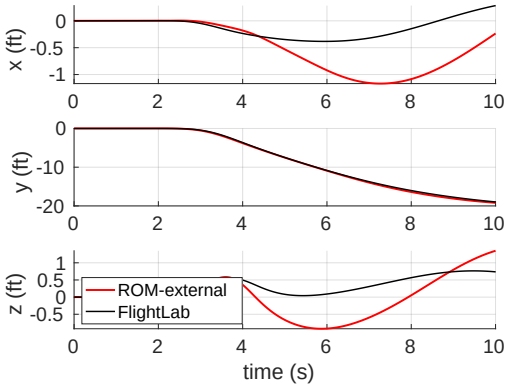

Figure 31: Low-gain controlled helicopter, trajectory response to θ_c, not-small perturbation input.

and FlightLab results is quite good in case of uncontrolled vehicle due to the difficulty of capturing the exact placement of the unstable poles, in the overall (for both kinematics and trajectory perturbations) the correlations become very good when the helicopter is controlled (particularly with the highest value of proportional gain). The comparison with FligthLab simulations prove that the ROM identified from controlled system data through the proposed algorithm provides quite accurate helicopter dynamics simulations (even in the presence of not-small perturbations) and, in particular, is capable of providing a reliable estimation of the effects produced by the actuation of an arbitrary controller. Therefore, the proposed modelling procedure can be efficiently applied for those design purposes which need the knowledge of the helicopter dynamics, like handling quality assessment and control law synthesis.

REFERENCES

[1] F. Nitzsche, C. Spieß, R. Leibbrandt, M. Gennaretti, G. Bernardini, J. Serafini, V. Riziotis, G. Papadakis, N. Spyropoulos, A. Siami, D. Hilewit, and M. Rafiee, "A new comprehensive analysis tool for the preliminary design and design evaluation of helicopters - the coral project," in *47th European Rotorcraft Forum, United Kingdom*, 7-9th September 2021.

[2] R. Gori, F. Pausilli, M. D. Pavel, and M. Gennaretti, "State-space rotor aeroelastic modeling for real-time helicopter flight simulation," in *Advanced Materials Research*, vol. 1016, pp. 451–459, Trans Tech Publ, 2014.

[3] M. Gennaretti and D. Muro, "Multiblade reduced-order aerodynamics for state-space aeroelastic modeling of rotors," *Journal of Guidanceircraft*, vol. 49, no. 2, pp. 495–502, 2012.

[4] M. Gennaretti, C. Pasquali, F. Cardito, J. Serafini, G. Bernardini, and R. Celi, "Dynamic wake inflow modeling in ground effect for flight dynamics applications," in *AHS 73nd Annual Forum & Technology Display*, 2017.

[5] C. R. Theodore, M. B. Tischler, and J. D. Colbourne, "Rapid frequency-domain modeling methods for unmanned aerial vehicle flight control applications," *Journal of Aircraft*, vol. 41, no. 4, pp. 735–743, 2004.

[6] M. B. Tischler and M. G. Cauffman, "Frequency-response method for rotorcraft system identification: flight applications to bo 105 coupled rotor/fuselage dynamics," *Journal of the American Helicopter Society*, vol. 37, no. 3, pp. 3–17, 1992.

[7] R. Gori, J. Serafini, M. Molica Colella, and M. Gennaretti, "Assessment of a state-space aeroelastic rotor model for rotorcraft flight dynamics," *CEAS Aeronautical Journal*, vol. 7, no. 3, pp. 405–418, 2016.

[8] A. Kuppusamy and S. J. Yoon, "Experimental flight testing and system identification of eurocopter as365n2 dauphin helicopter using cifer®," *International Journal of Applied Engineering Research*, vol. 12, no. 24, pp. 14287–14298, 2017.

[9] H.-J. Ahn, S.-W. Lee, S.-H. Lee, and D.-C. Han, "Frequency domain control-relevant identification of mimo amb rigid rotor," *Automatica*, vol. 39, no. 2, pp. 299–307, 2003.

[10] R. Mandloi and P. Shah, "Methods for closed loop system identification in industry," *Journal of Chemical and Pharmaceutical Research*, vol. 7, no. 1, pp. 892–896, 2015.

[11] D. S. Miller, *Open loop system identification of a micro quadrotor helicopter from closed loop data*. University of Maryland, College Park, 2011.

[12] J. S. Bendat and A. G. Piersol, *Random data analysis and measurement procedures*. IOP Publishing, 2000.

[13] M. B. Tischler and R. K. Remple, *Aircraft and rotorcraft system identification*. American Institute of Aeronautics and Astronautics Reston, VA, 2012.

[14] R. K. Otnes, "Applied time series analysis," *V. 1 Basic Techniques*, vol. 449, 1978.

[15] R. Du Val and C. He, "Flightlab tm modeling for real-time simulation applications," *International Journal of Modeling, Simulation, and Scientific Computing*, vol. 8, no. 04, p. 1743003, 2017.

[16] G. D. Padfield, *Helicopter Flight Dynamics*. Blackwell Science Ltd, 1996.